ELSEVIER

Journal of Power Sources 81–82 (1999) 547–553

JOURNAL OF POWER SOURCES

www.elsevier.com/locate/jpowsour

X-ray diffraction, ^{57}Fe Mössbauer and step potential electrochemical spectroscopy study of $LiFe_yCo_{1-y}O_2$ compounds

R. Alcántara [a,*], J.C. Jumas [b], P. Lavela [a], J. Olivier-Fourcade [b], C. Pérez-Vicente [b], J.L. Tirado [a]

[a] *Laboratorio de Química Inorgánica, Facultad de Ciencias, Universidad de Córdoba, Avda. San Alberto Magno s / n, 14004 Cordova, Spain*
[b] *Laboratoire de Physicochimie de la Matière Condensée (UMR 5617 CNRS), CC-003, Université Montpellier II, Place Eugène Bataillon, 34095 Montpellier Cedex 5, France*

Abstract

With the aim of finding new cathode materials for lithium-ion batteries, the synthesis of layered solid solutions with $LiFe_yCo_{1-y}O_2$ stoichiometries has been studied in this work. X-ray single phase products were obtained by a ceramic procedure for $0 \leq y \leq 0.2$. The unit cell dimensions of the powdered solids increase with the iron content. The Rietveld analysis of a sample with $y = 0.1$ using anisotropic thermal parameters led to $R_{BRAGG} = 3.37$. The hexagonal unit cell parameters of this solid were $a = 2.8271(1)$ Å and $c = 14.1266(7)$ Å. The site occupancy used in the Rietveld procedure was: $(Fe^{T}_{0.0086})_{6c}[Li_{0.9868}Fe^{O}_{0.0046}]_{3b}[Li_{0.0132}Co_{0.9000}Fe^{O}_{0.0868}]_{3a}O_2$ according to the intensity of the signals observed in the Mössbauer spectrum. This consists of one intense (87%) quadrupole split signal with isomer shift of ca. 0.316(3) mm/s is ascribable to Fe(III) replacing cobalt in the CoO_2 layers. Two weaker quadrupole signals result from small amounts of iron in octahedral 3b and pseudotetrahedral 6c sites of the LiO_2 layers. The presence of pseudotetrahedral iron puts obstacles to the lithium ion diffusivity. In consequence, the electrochemical spectra evidence an increased cell polarization as increases. The lithium extraction at the end of the first charge decreases with iron content, with a maximum of 0.6 Li per formula for $y = 0.1$. The introduction of nickel in the composition of these solids may be useful to improve the electrochemical performance of the solid solutions. Ternary systems show an improved electrochemical behaviour.

Keywords: Lithium battery; Lithium-ion batteries; Lithium cobalt oxide; Lithium iron oxide; ^{57}Fe Mössbauer spectroscopy

1. Introduction

Although $LiFeO_2$ crystallizes in three non-layered structures, and was not found in a layered phase until recently [1], most lithium-trivalent metal oxides, $LiMO_2$ possess a rhombohedral structure close to α-$NaFeO_2$. One relevant example is $LiCoO_2$, an extensively studied solid, as a result of being the first active cathode material in a commercial lithium-ion cell. In consequence, different solid solutions with layered structures have been tested as active material in the preparation of intercalation electrodes for advanced batteries. Unfortunately, a net improvement in the electrochemical performance of the electrodes is not always observed. Nevertheless, partial substitution of Co by Ni, Cr and Al and substitution of Ni in $LiNiO_2$ by Fe, Mn and Al have been reported.

The preparation and characterization of homogeneous $LiNi_{1-y}Co_yO_2$ compounds with $(0 \leq y \leq 1)$ was first reported by Ohzuku et al. [2] and studied in detail by Delmas and Saadoune [3], Gummow and Thackeray [4], and others [5,6]. $LiCr_yCo_{1-y}O_2$ was obtained by Jones et al. [7]. Recently, the preparation of solid solutions of the $LiAlO_2$–$LiCoO_2$ system in the complete composition range was reported [8].

On the other hand, Reimers et al. [9] reported a detailed study of $LiFe_yNi_{1-y}O_2$ solids, in which electrochemical measurements carried out in lithium cells showed that the amount of lithium that could be reversibly cycled decreased with y. Similar results were also obtained by Kanno et al. [10]. $Li_xMn_yNi_{1-y}O_2$ was studied by Rossen et al. [11] and Caurant et al. [12]. The synthesis of a single phase products with $LiAl_yNi_{1-y}O_2$ was reported by Zhong and von Sacken [13] and Ohzuku et al. [14].

With the aim of finding new cathode materials for lithium-ion batteries, the synthesis, structural characteriza-

* Corresponding author. Tel.: +34-957-218637; Fax: +34-957-218606; E-mail: iqlticoj@lucano.uco.es

0378-7753/99/$ - see front matter
PII: S0378-7753(99)00213-X

tion and application in lithium cells of layered solid solutions with $LiFe_yCo_{1-y}O_2$ stoichiometries are studied in this work.

2. Experimental

Lithium-transition metal mixed oxides $LiFe_yCo_{1-y}O_2$ $(0 \le y \le 1)$ with different nominal compositions were prepared by heating stoichiometric amounts of LiOH, Fe_2O_3 and Co_3O_4. The parent solids were intimately mixed by prolonged grinding, pressed into pellets and heat treated at 800°C for 24 h in an air atmosphere. A powder sample with $LiFe_{0.1}Ni_{0.7}Co_{0.2}O_2$ stoichiometry was obtained by adding NiO in appropriate proportion, which was obtained by the in situ thermal decomposition of $Ni(NO_3)_2$, and a small excess lithium hydroxide amount.

X-ray powder diffraction data (XPD) were obtained with a Siemens D5000 apparatus provided with CuK_α radiation and graphite monochromator. Step-scan recordings for structure refinement by the Rietveld method were carried out by using $0.04°2\theta$ steps of 12-s duration. The computer program DBWS9000 was used in the calculations [15]. FTIR transmittance spectra were obtained with a BOMEM apparatus, using KBr pellets.

^{57}Fe Mössbauer spectra of the samples were obtained at room temperature with an ELSCINT AME 40 constant acceleration spectrometer. The source was ^{57}Co in a Rh matrix. The velocity scale was calibrated by using the magnetic sextet spectrum of a high purity iron foil absorber. Recorded spectra were fitted to Lorentzian profiles by least square method [16] and the fit quality was controlled by the classical χ^2. The origin of the isomer shift scale was determined from the center of the α-Fe spectra, also recorded at room temperature.

The electrochemical performance of $Li/LiClO_4$(PC + EC)/mixed oxide test cells was studied in galvanostatic and potentiostatic modes by using a multichannel 'MacPile' system [17]. Cell cathodes were prepared by pressing at ca. 4 tons, a mixture of 82% of active material, 12% 4N carbon black (Strem) and 6% EPDM binder. Step potential electrochemical spectroscopy (SPES) was carried out with 10 mV/h steps after an initial relaxation of the cell until the condition $\Delta V/\Delta t < 1$ mV/h. Galvanostatic cycling was performed in the as-prepared cells at C/50 and C/100 (i.e., allowing a $\Delta x = 1$ in Li_xCoO_2 in 50 and 100 h, respectively).

3. Results and discussion

X-ray single phase $LiFe_yCo_{1-y}O_2$ products were obtained for $0 \le y \le 0.2$. For $y > 0.2$, a set of lines corresponding to a new crystalline modification isostructural with cubic α-$LiFeO_2$ increase progressively in intensity and becomes the most intense X-ray diffraction signals for $y \ge 0.8$. Moreover, for $y \ge 0.3$, the occurrence of low-intensity diffraction lines ascribable to Fe_3O_4 was detected. The occurrence of biphase cubic/hexagonal products was also found in $LiFe_yNi_{1-y}O_2$ for $y > 0.23$ by Reimers et al. [9]. For the X-ray single phase products, the diffraction patterns could be indexed in a $R\bar{3}m$ lattice (Fig. 1). The unit cell parameters of the layered phase present in all samples were refined and plotted vs. y (Fig. 2). Up to $y = 0.3$, a clear increase in both a and c parameters is observed which evidences the expansion of the unit cell volume to accommodate the larger high-spin Fe^{3+} ions [18] in the structure of $LiCoO_2$. Larger iron contents do not lead to a net expansion in a, while the c parameter decreases slightly. This behaviour is probably associated to the occurrence of two different processes: metal substitution following a trend such as that expected by the Vegard's law for y values below 0.4 and the occupancy of different sites or formation of new phases for higher y. Fig. 2 also includes a plot of the c/a ratio vs. composition which shows a pronounced increase after the introduction of small amounts of iron in the structure.

Fig. 3 shows the FTIR spectra of $LiCoO_2$ and four iron-containing compositions. As previously reported, four bands are expected in the CoO_6 region of the spectra of layered $LiCoO_2$, although the resolution of the bands depends markedly on the previous history of the sample [19]. On the contrary, Preudhomme [20] showed that the number of bands for a cation-disordered spinel is two. The experimental spectra in Fig. 3 evidence that the three

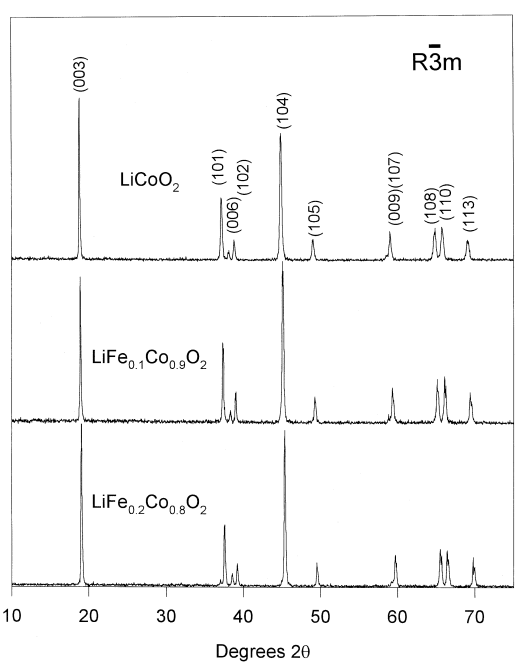

Fig. 1. X-ray diffraction patterns of solids with $LiFe_yCo_{1-y}O_2$ nominal stoichiometries showing $R\bar{3}m$ Miller indices.

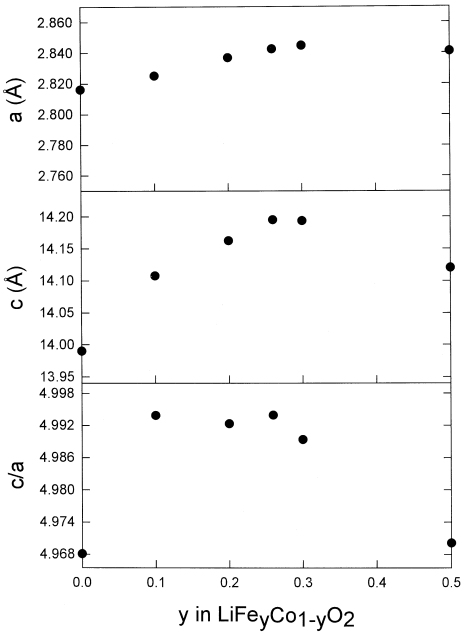

Fig. 2. Evolution of the hexagonal unit cell parameters with the composition y of $LiFe_yCo_{1-y}O_2$ solids.

well-resolved bands in iron-free sample change their wavenumber significantly with transition metal substitution. However, the increase in wavenumber observed for $y = 0.1$, leads to lower values for higher iron contents. This evolution is comparable to that previously discussed on the unit cell parameters and evidences that a solid solution model is only acceptable below $y = 0.3$. Moreover, for larger iron contents ($y = 0.8$ in Fig. 3) the bands are no longer resolved and the spectra trends to that of cubic α-$LiFeO_2$.

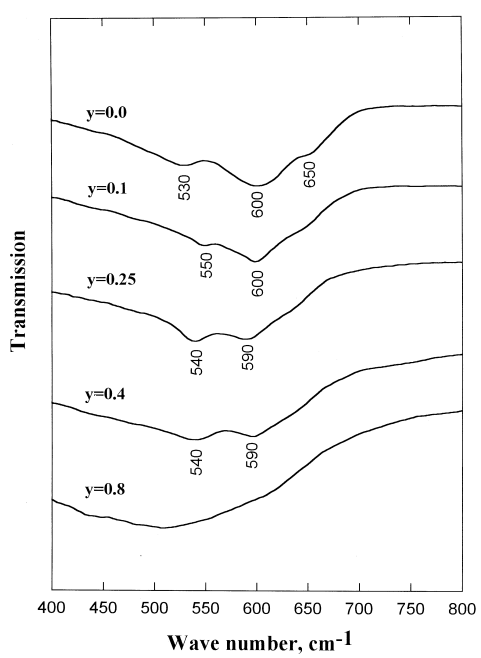

Fig. 3. FTIR spectra of $LiFe_yCo_{1-y}O_2$ solids.

Fig. 4 shows the Mössbauer spectra of the samples with $LiFe_yCo_{1-y}O_2$ stoichiometry. One intense (87%) quadrupole split signal with isomer shift of ca. 0.316(3) mm/s is ascribable to Fe(III) replacing cobalt in the CoO_2 layers. Two weaker quadrupole signals result from small amounts of iron in octahedral and pseudotetrahedral sites of the LiO_2 layers. This iron content probably leads to a poorer reversibility of the lithium extraction–insertion process. The quantitative evaluation of the spectra in Fig. 4 leads to the parameters which are collected in Table 1. It can be observed that the relative intensity of tetrahedral

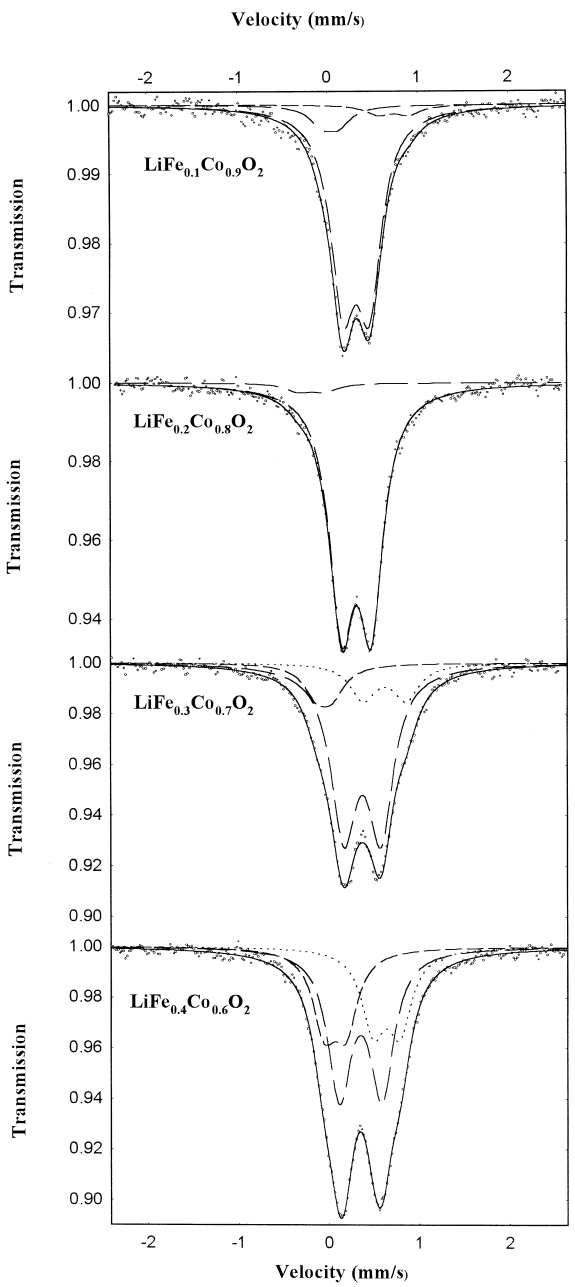

Fig. 4. Experimental spectra (dots), calculated (full line) and component signals (dotted lines) in the ^{57}Fe Mössbauer spectra of $LiFe_yCo_{1-y}O_2$ solids.

Table 1
^{57}Fe Mössbauer parameters of the calculated signals in the spectra of $LiFe_yCo_{1-y}O_2$ solids

Sample comp. y	Isomer shift (mm/s)	Quadrupole splitting (mm/s)	Line-width (mm/s)	Contribution (%)
Central doublet				
0.1	0.316 (3)	0.290 (4)	0.326 (9)	86.8
0.2	0.311 (2)	0.325 (3)	0.326 (4)	96.5
0.3	0.373 (3)	0.409 (5)	0.340 (9)	71.9
0.4	0.351 (3)	0.470 (7)	0.31 (2)	49.0
Doublet at high mm / s				
0.1	0.73 (5)	0.33 (5)	0.326 (9)	4.6
0.2	–	–	–	–
0.3	0.62 (1)	0.47 (2)	0.340 (9)	15.8
0.4	0.638 (7)	0.29 (1)	0.31 (2)	26.0
Doublet at low mm / s				
0.1	0.04 (3)	0.18 (1)	0.326 (9)	8.6
0.2	−0.18 (7)	0.29 (6)	0.326 (4)	3.5
0.3	−0.05 (2)	0.17 (2)	0.340 (9)	12.3
0.4	0.07 (9)	0.24 (1)	0.31 (2)	25.0

iron increases dramatically above $y = 0.3$, revealing the complete switch from a simple solid solution model. Undoubtedly, the occurrence of Fe_3O_4 and $LiFeO_2$ side products could have a significant effect on the Mössbauer spectra. In fact, the Mössbauer parameters corresponding to α-$LiFeO_2$ ($\delta = 0.5$ mm/s and $\Delta = 0.28$ mm/s) [21] agree fairly well with those of the high doublet at higher intensity for $LiFe_{0.4}Co_{0.6}O_2$.

The Rietveld analysis of the X-ray diffraction pattern of a sample with $Li(Fe_{0.1}Co_{0.9})O_2$ stoichiometry (Fig. 5) was carried out by using anisotropic thermal parameters, and led to $R_{BRAGG} = 3.37$ (Table 2). The hexagonal unit cell parameters of this solid were $a = 2.8271(1)$ Å and $c = 14.1266(7)$ Å. The site occupancies of iron atoms used in the refinement were those obtained from the Mössbauer spectra (Table 1). The Li/(Fe + Co) and Fe/Co ratios were imposed by the chemical composition of the solid. Attempts to allow varying these occupancy values during the Rietveld refinement did not improve the R_{BRAGG} values. Thus, the final Rietveld cation distribution was considered to be: $(Fe^{T}_{0.0086})_{6c}[Li_{0.9868}Fe^{O}_{0.0046}]_{3b}[Li_{0.0132}Co_{0.9000}Fe^{O}_{0.0868}]_{3a}O_2$. The error associated to the occu-

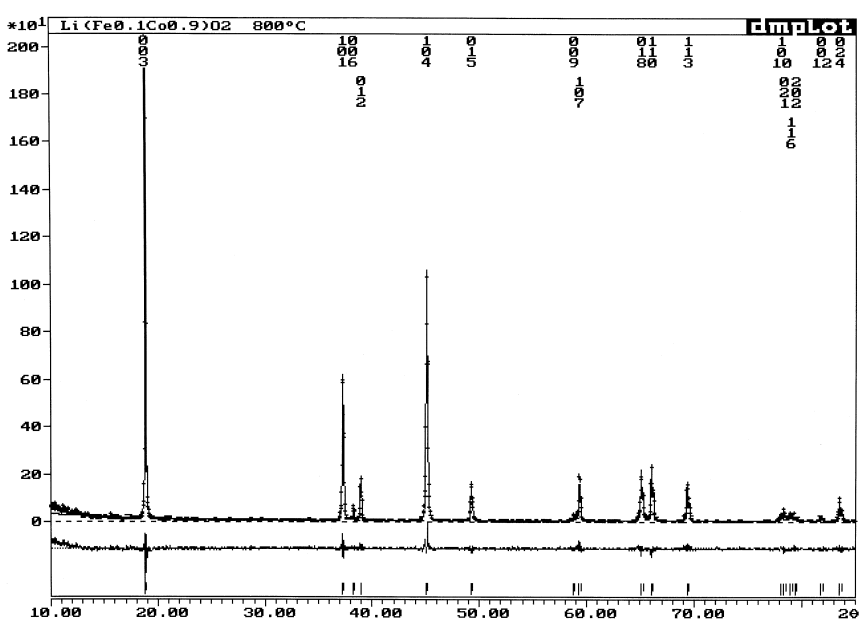

Fig. 5. Experimental (crosses), calculated (full line) and difference (below) patterns resulting from the Rietveld refinement of X-ray diffraction data of $LiFe_{0.1}Co_{0.9}O_2$.

Table 2
Results of the Rietveld refinement of powder X-ray diffraction data for $LiFe_{0.1}Co_{0.9}O_2$

Nominal composition	$LiFe_{0.1}Co_{0.9}O_2$
Space group	$R\bar{3}m$
Hexagonal axes	
a, Å	2.8271 (1)
c, Å	4.1266 (7)
Z	3
Temp, K	298
Radiation	CuK_α
2θ limits, deg	16–110
R_B	3.37
$S\ (R_w/R_e)$	1.16

Fractional coordinate

Atom	Site	x	y	z	Occupancy
Co	3a	0.0	0.0	0.0	0.9000
Fe(1)	3a	0.0	0.0	0.0	0.0868
Li(1)	3a	0.0	0.0	0.0	0.0132
Li(2)	3b	0.0	0.0	0.5	0.9868
Fe(2)	3b	0.0	0.0	0.5	0.0046
O	6c	0.0	0.0	0.2600 (6)	2.000
Fe(3)	6c	0.0	0.0	0.450 (6)	0.0086

Cation distribution: $(Fe^{T}_{0.0086})_{6c}[Li_{0.9868}Fe^{O}_{0.0046}]_{3b}[Li_{0.0132}Co_{0.9000}Fe^{O}_{0.0868}]_{3a}O_2$.

pancy of equivalent sites by iron atoms is then the same of the refinement of ^{57}Fe Mössbauer spectra (Fig. 4).

SPES results (Fig. 6) evidence several differences with respect to pure HT-$LiCoO_2$. In the latter, the main oxidation peak is placed at ca. 3.98 V, while for all the iron–cobalt samples studied in this work, the same signal has a maximum located at a slightly higher potential than 4.0 V (ca. 4.06 V). This small cell voltage polarization can be related with a continuous decrease of the peak intensity as the iron content is increased. The maximum lithium extraction, 0.6 Li per formula, after the first charge at 4.1 V was observed for $y = 0.1$, although lithium intercalation

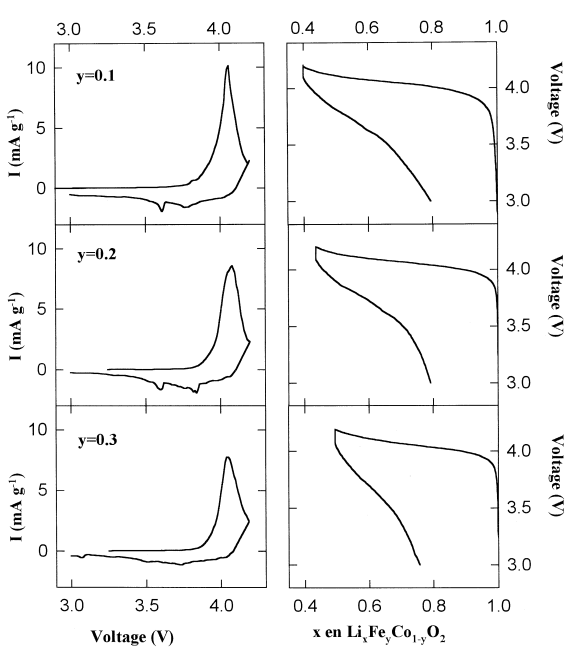

Fig. 6. Intensity vs. voltage (left) and voltage vs. composition, x (right) obtained by SPES of lithium cells using $Li_xFe_yCo_{1-y}O_2$ electrodes with different iron content, y.

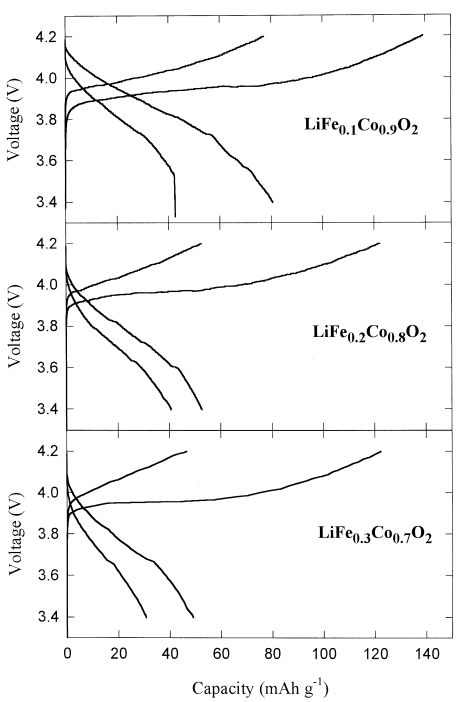

Fig. 7. Galvanostatic charge–discharge cycles of lithium cells using $Li_xFe_yCo_{1-y}O_2$ electrodes with different iron content, y.

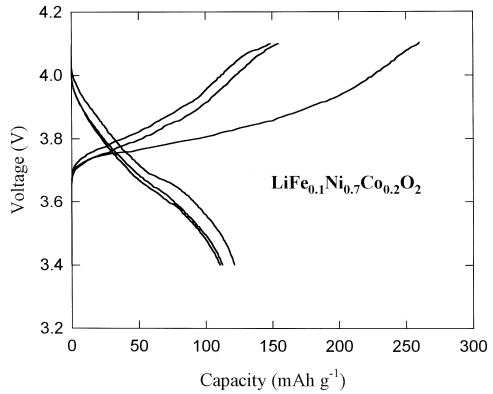

Fig. 8. Galvanostatic charge–discharge cycles of a lithium cell using $LiFe_{0.1}Ni_{0.7}Co_{0.2}O_2$ electrode.

only allowed to recover 0.4 Li per formula at 3.0 V in the first discharge. For higher iron contents, the performance of the electrodes decreases progressively.

For the discharge reaction under potentiostatic conditions (Fig. 6), a low reversibility was evidenced, as a consequence of the extremely low intensity of the measured reduction peak at ca. 3.85 V. An additional feature is the presence of very low intense oxidation and reduction signals in samples with $y = 0.1$ and 0.2 stoichiometries. These peaks are located at ca. 3.9 and 3.6 V, respectively. These voltage values could be in agreement with the presence of an almost negligible quantity of spinel-related phase or a phase structurally similar to the low temperature modification of $LiCoO_2$ [22]. However, its low content make these possible impurity phases undetectable by X-ray diffraction. The presence of LT modifications is in contradiction with the fact that efforts to obtain an iron-containing LT modification at their typical temperature (400–500°C) were unsuccessful. Moreover, the presence of tetrahedral iron as content increases can be considered as indicative of the progressive conversion to an spinel-related solid.

The first two galvanostatic charge and discharge curves are shown in Fig. 7. A kinetic effect is evidenced by the enhanced polarization found for the first cycle. This phenomenon can be considered as a consequence of a poorer lithium ion diffusivity, resulting from the presence of iron in both tetrahedral and octahedral sites of the lithium layers, as discussed above. In summary, the progressive deterioration of the electrochemical behaviour of the $LiFe_yCo_{1-y}O_2$ compositions could be interpreted in terms of cation distribution derived from the analysis of X-ray diffraction patterns and Mössbauer spectra.

As found in $LiCoO_2$ [2–4,19] and $LiAl_yCo_{1-y}O_2$ [8], the addition of nickel to the composition of the mixed oxides may improve the electrochemical performance of the cathode materials. In fact, pure $LiNiO_2$ commonly displays a more extended reversible deintercalation than $LiCoO_2$. Ternary $LiFe_xNi_yCo_zO_2$ systems are now under evaluation. Up to now, nickel has been incorporated in the stoichiometry of the $LiFe_yCo_{1-y}O_2$ solid solutions by using the ceramic preparative procedure described in Section 2, leading to a final $LiFe_{0.1}Ni_{0.7}Co_{0.2}O_2$ stoichiometry. The unit cell parameters of this solid were $a = 2.8728(7)$ Å and $c = 14.226(7)$ Å. The c/a ratio (4.94) reveals a less marked trigonal distortion as compared with the results for $LiFe_yCo_{1-y}O_2$ solid, shown in Fig. 2. The divergences between the unit cell parameters of $LiFe_{0.1}Ni_{0.7}Co_{0.2}O_2$ and those reported for $LiFe_{0.1}Ni_{0.9}O_2$ [9] and $LiFe_{0.1}Co_{0.9}O_2$ (Fig. 2) are probably indicative of a different cation distribution and, in consequence, a different electrochemical behaviour, now induced by the simultaneous presence of cobalt and nickel in the structure of the solid. The preliminary electrochemical results of lithium cells using these novel cathode materials are shown in Fig. 8. The first galvanostatic cycles evidence a larger capacity and a better reversibility of the lithium extraction–insertion process of $LiFe_{0.1}Ni_{0.7}Co_{0.2}O_2$, as compared with the $LiFe_{0.1}Co_{0.9}O_2$ electrode (Fig. 7). A capacity of ca. 120 mAh g^{-1} is retained after the fourth cycle.

Acknowledgements

The authors are indebted to the European Commission (Contracts No. ERBFMBICT 96.0768 and ERBFMBICT 983020), CNRS and Universidad de Córdoba.

References

[1] R. Kanno, T. Shirane, Y. Kawamoto, Y. Takeda, M. Takano, M. Ohashi, Y. Yamaguchi, J. Electrochem. Soc. 143 (1996) 2435.
[2] T. Ohzuku, H. Komori, K. Swai, T. Hirai, Chem. Express 5 (1990) 733.
[3] C. Delmas, I. Saadoune, Solid State Ionics 53–56 (1992) 370.
[4] R.J. Gummow, M.M. Thackeray, Solid State Ionics 53–56 (1992) 681.
[5] D. Caurant, N. Baffier, B. Garcia, J.P. Pereira-Ramos, Solid State Ionics 91 (1996) 45.
[6] R. Alcántara, P. Lavela, J.L. Tirado, E. Zhecheva, R. Stoyanova, J. Electrochem. Soc. 145 (1998) 730.
[7] C.D.W. Jones, E. Rossen, J.R. Dahn, Solid State Ionics 68 (1994) 65.
[8] R. Alcántara, P. Lavela, P.L. Relaño, J.L. Tirado, E. Zhecheva, R. Stoyanova, Inorg. Chem. 37 (1998) 264.
[9] J.N. Reimers, E. Rossen, C.D. Jones, J.R. Dahn, Solid State Ionics 61 (1993) 335.
[10] R. Kanno, T. Shirane, Y. Inaba, Y. Kawamoto, J. Power Sources 68 (1997) 145.
[11] E. Rossen, C.W.D. Jones, J.R. Dahn, Solid State Ionics 57 (1992) 311.
[12] D. Caurant, N. Baffier, V. Bianchi, G. Grégoire, S. Bach, J. Mater. Chem. 6 (1996) 1149.
[13] Q. Zhong, U. von Sacken, J. Power Sources 54 (1995) 221.
[14] T. Ohzuku, A. Ueda, M. Kouguchi, J. Electrochem. Soc. 142 (1995) 4033.
[15] R.A. Young, D.B. Wiles, J. Appl. Crystallogr. 15 (1982) 430.

[16] W. Kündig, Nucl. Instr. and Meth. 75 (1969) 336.
[17] Y. Chabre, D. Djurado, M. Armand, W.R. Romanow, N. Coustel, J.P. McCauley, J.E. Fischer, A.B. Smith, J. Am. Chem. Soc. 114 (1992) 764.
[18] R.D. Shannon, Acta Cryst. A 32 (1976) 751.
[19] J. Morales, R. Stoyanova, J.L. Tirado, E. Zhecheva, J. Solid State Chem. 113 (1994) 182.
[20] J. Preudhomme, Ann. Chim. 9 (1974) 31.
[21] M. Georges, A. Fatseas, S. Lefebvre, C.R. Acad. Sci. Paris 266 (1968) 374.
[22] B. Garcia, J. Farcy, J.P. Pereira-Ramos, N. Baffier, J. Electrochem. Soc. 144 (1997) 1179.